Preparation and Dielectric Characterization of P(VDF-TrFE) Copolymer-Based Composites Containing Metal-Formate Frameworks

Šimenas, Mantas; Balčiu Nas, Sergejus; Gonzalez-Nelson, Adrian; Kinka, Martynas; Ptak, Maciej; Van Der Veen, Monique A.; Maczka, Mirosław; Banys, Ju Ras

DOI
10.1021/acs.jpcc.9b04235

Publication date
2019

Document Version
Final published version

Published in
Journal of Physical Chemistry C

THE JOURNAL OF PHYSICAL CHEMISTRY C

Article

Cite This: J. Phys. Chem. C 2019, 123, 16380−16387

pubs.acs.org/JPCC

Preparation and Dielectric Characterization of P(VDF−TrFE) Copolymer-Based Composites Containing Metal−Formate Frameworks

Mantas Šimėnas,*[,†] Sergejus Balčiūnas,[†] Adrian Gonzalez-Nelson,[‡,§] Martynas Kinka,[†] Maciej Ptak,[∥] Monique A. van der Veen,[‡] Mirosław Mączka,[∥] and Jūras Banys[†]

[†]Faculty of Physics, Vilnius University, Sauletekio av. 9, LT-10222 Vilnius, Lithuania

[‡]Catalysis Engineering, Department of Chemical Engineering, Delft University of Technology, van der Maasweg 9, 2629 HZ Delft, The Netherlands

[§]DPI, P.O. Box-902, 5600 AX Eindhoven, The Netherlands

[∥]Institute of Low Temperature and Structure Research, Polish Academy of Sciences, P.O. Box-1410, PL-50-950 Wroclaw 2, Poland

Supporting Information

ABSTRACT: We report the synthesis and dielectric characterization of novel polyvinylidene fluoride−trifluoroethylene P(VDF−TrFE) composite films containing $[(CH_3)_2NH_2][Mg(HCOO)_3]$ (DMAMg) and $[NH_4][Zn(HCOO)_3]$ (AmZn) dense metal−organic frameworks (MOFs). The optical camera and Raman microscopies are used to map the distribution of the MOF fillers in the prepared films. The dielectric spectroscopy experiments of the DMAMg/P(VDF−TrFE) composite performed in a broad temperature range demonstrate rich dielectric behavior originating from the dipolar dynamics of the $(CH_3)_2NH_2^+$ molecular cations and glassy behavior of the copolymer matrix. An anomalous behavior of the complex dielectric permittivity is also observed because of the structural phase transition of DMAMg fillers. The dielectric properties of the AmZn/P(VDF−TrFE) composite film are mainly determined by the dipolar glass relaxation of the P(VDF−TrFE) polymer. The frequency-dependent dielectric spectra of both composites allow us to characterize the observed dipolar relaxation processes. The $(CH_3)_2NH_2^+$ cation dynamics follows the Arrhenius law, whereas the glassy behavior of P(VDF−TrFE) is described by the Vogel−Fulcher equation. For both composites, we observe a significant increase of the dielectric permittivity compared with the P(VDF−TrFE) film without MOF fillers.

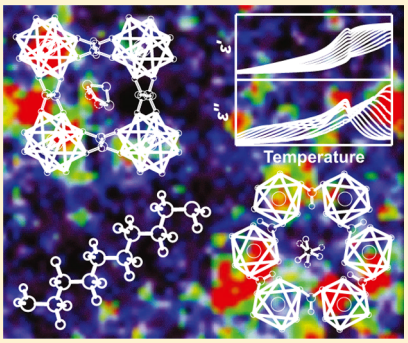

INTRODUCTION

Metal−organic frameworks (MOFs) are an emerging subclass of hybrid materials composed of metal centers that are joined together by organic linkers into highly porous structures.[1−3] The pronounced MOF porosity can be utilized for gas adsorption[4] and related applications such as gas storage,[5,6] separation,[7] and drug delivery.[8] In addition to the ordinary frameworks, over the past decade, a new hybrid family of dense MOFs also received considerable attention.[9−14]

The most popular dense MOFs are metal−formate frameworks $[A][M(HCOO_3)]$ consisting of transition metal or magnesium centers linked by formate $HCOO^-$ anions into structures with regular nanocages.[10−12,15] Each such pore contains a single molecular cation A^+, which usually shows dynamic behavior at room temperature.[16,17] The majority of formate frameworks exhibit structural phase transitions, during which the cation motion ceases and a long-range order is established.[10,15,18] In some cases, the ordered phases are pyroelectric[15,19−21] or even ferroelectric.[12,22] The magnetic analogues of formate frameworks also exhibit magnetic ordering at temperature below 40 K,[23,24] making these materials potential single structural phase multiferroics,[11,15] which is a very rare and highly desirable material property.[25]

The dimethylammonium metal−formate frameworks $[(CH_3)_2NH_2][M(HCOO)_3]$ (DMAM, where M = Zn, Cu, Ni, Co, Fe, Mn, and Mg) constitute the most thoroughly studied family of $[A][M(HCOO_3)]$ compounds.[10,11,26] All members except for DMACu[27] exhibit a single structural phase transition, which involves cooperative ordering of the DMA^+ cations inside the cuboid metal−formate cages (see Figure 1a).[28] In the high-temperature disordered phase, the molecular cations are constantly hopping between three favorable states, whereas in the low-temperature phase, they occupy a single position.[18] The phase transition temperature T_0 of DMAM depends on the metal center, and for compounds with the transition metal ions, it is within the 155−190 K temperature range.[10,11] The DMAMg framework shows exceptionally high T_0 of about 260 K, making this compound more attractive for

Received: May 4, 2019
Revised: June 5, 2019
Published: June 12, 2019

DOI: 10.1021/acs.jpcc.9b04235
J. Phys. Chem. C 2019, 123, 16380−16387

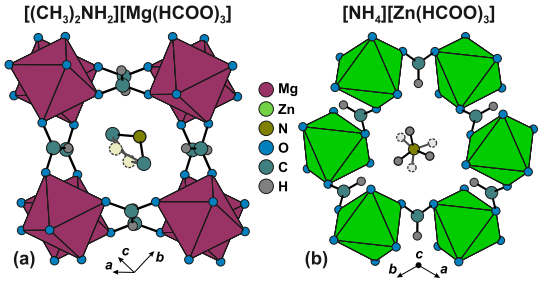

Figure 1. Crystal structures of (a) DMAMg[28] and (b) AmZn[12] frameworks in the high-temperature phases. The dashed atoms mark equivalent positions of the molecular cations. Hydrogen atoms of the DMA^+ cation are omitted for clarity.

applications concerning its dielectric properties.[26,29,30] The ferroelectric nature of these materials was only demonstrated for the deuterated DMACo,[22] while recent studies raised doubts about the ferroelectric origin of DMAZn.[31,32]

A clear ferroelectric behavior below T_0 = 191 K was revealed for chiral ammonium zinc-formate framework $[NH_4][Zn(HCOO)_3]$ (AmZn).[12,24] In this compound, the Am^+ cations are situated within the hexagonal channel-like cages and exhibit a twofold disorder in the high-temperature phase (see Figure 1b). Similar to the DMAM family, in the ordered phase, the ammonium cations occupy a single position causing the long-range ferroelectric order.[12]

Recently, various MOFs have also been embedded in the polymer matrices to produce functional MOF/polymer composites.[33−37] Among such composites, the so-called mixed-matrix membranes with various MOF fillers received exceptional attention because of the enhanced gas separation properties.[36,38,39] Several studies also reported a successful inclusion of several different MOFs in the ferroelectric polyvinylidene fluoride (PVDF) polymer matrix.[40−43] However, none of these studies report dielectric characterization of these composites.

In general, composites based on PVDF or its copolymer with trifluoroethylene P(VDF−TrFE) with embedded electrically active inorganic fillers show exceptional promise for applications in various devices such as capacitors, actuators, sensors, and contact switches.[44−48] The films of the P(VDF−TrFE) polymer itself offer relatively good mechanical compliance, ferroelectric, pyroelectric, and piezoelectric properties compared with other polymers.[49] P(VDF−TrFE) copolymer with the molar ratio of 70/30 is one of the most studied compositions. It has a high degree of crystallinity and reversible ferroelectric phase transition at about 380 K on heating.[46]

In this study, for the first time, we combine peculiar dielectric properties of metal−formate frameworks and P(VDF−TrFE) copolymer by preparing and characterizing DMAMg/P(VDF−TrFE) and AmZn/P(VDF−TrFE) composites. The obtained free-standing films are studied by Raman and dielectric spectroscopies, revealing rich dielectric behavior stemming from the respective constituents of both composites.

SAMPLE PREPARATION AND EXPERIMENTAL DETAILS

Synthesis of DMAMg and AmZn. $MgCl_2$ (98%, Sigma-Aldrich), $ZnCl_2$ (98%, Fluka), NH_4HCOO (99%, Fluka), 2.0 M solution of $(CH_3)_2NH$ in methanol (Sigma-Aldrich), methanol (99.8%, Sigma-Aldrich), and formic acid (98%, Fluka) were commercially available and used without further purification. DMAMg was obtained by a slow diffusion method. In a typical experiment, 16 mL of methanol solution containing 12.8 mmol of $(CH_3)_2NH$ and 12.8 mmol of formic acid was placed at the bottom of a glass tube (9 mm inner diameter). On this solution, 16 mL of methanol solution containing 2 mmol of $MgCl_2$ was gently added. The tube was sealed and kept undisturbed. Colorless crystals were harvested after 5 days.

The same slow diffusion method was used to obtain AmZn, but the solution placed at the bottom of a glass tube contained 16 mL of methanol, 12.8 mmol of NH_4HCOO, and 12.8 mmol of formic acid, whereas the solution placed above contained 2 mmol of $ZnCl_2$ dissolved in 16 mL of methanol. Colorless crystals were harvested after 1 week.

Preparation of Composites. DMAMg/P(VDF−TrFE) film: a polymer solution was prepared by stirring 200 mg of P(VDF−TrFE) (70/30% mol, Piezotech) in 2 mL of anhydrous *N*,*N*-dimethylformamide (DMF) for 1 h. Ground crystals of DMAMg (60 mg) were added to the polymer solution, and the mixture was stirred for additional 80 min. The vial was then placed in an ultrasonication bath for 20 min, followed by 10 min of stirring. The suspension was cast on a glass slide using a doctor blade set to 70 μm. The film was dried in a vacuum oven at 55 °C for 16 h. The MOF content in the DMAMg/P(VDF−TrFE) film is 23 wt %, estimated from the amounts present in the casting suspension.

AmZn/P(VDF−TrFE) film: a polymer solution was prepared by stirring 200 mg of P(VDF−TrFE) (70/30% mol, Piezotech) in 2 mL anhydrous DMF for 1 h. Ground crystals of AmZn (40 mg) were then added to the polymer solution, and the mixture was stirred for additional 80 min. The vial was then placed in an ultrasonication bath for 20 min, followed by 10 min of stirring. The suspension was cast on a glass slide using a doctor blade set to 60 μm. The freshly cast film was kept in a closed container with dry silica gel to reduce exposure to humidity. The film was dried in a vacuum oven at 55 °C for 16 h. The MOF content in the AmZn/P(VDF−TrFE) film is 17 wt %.

Blank P(VDF−TrFE) film: P(VDF−TrFE) (70/30% mol, Piezotech) film without inclusions was prepared by dissolving 260 mg of the polymer in 2 mL of DMF and casting with a doctor blade set to 90 μm. The film was dried in a vacuum oven at 55 °C for 16 h.

Raman Spectroscopy. Raman spectra were measured in the 50−3500 cm^{-1} range using a Renishaw inVia Raman microscope equipped with a confocal DM 2500 Leica optical microscope, a thermoelectrically cooled CCD as a detector, and an argon laser operating at 488 nm. A 20×/0.4 microscope magnification lens was used, spectra were collected using five accumulations and acquisition time of 25 s. A composite film was placed between two microscope glass slides to focus the laser beam on the surface of the film and perform mapping. Maps were generated using Wire 3.4 (Renishaw) by analyzing the intensity (height after subtraction of a linear baseline) of peaks at 2868 cm^{-1} (DMAMg/P(VDF−TrFE) film) and 1370 cm^{-1} (AmZn/P(VDF−TrFE) film). Maps were collected by taking the Raman spectra in the 2700−3240 cm^{-1} DMAMg/P(VDF−TrFE) and 1010−1700 cm^{-1} AmZn/P(VDF−TrFE) ranges measured with 5 μm step in both x and y directions over 300 μm × 350 μm area. A 20×/0.4 microscope magnification lens was used, and spectra were collected using

DOI: 10.1021/acs.jpcc.9b04235
J. Phys. Chem. C 2019, 123, 16380−16387

one accumulation and acquisition time of 3 s. The laser spot diameter was about 0.75 μm.

Dielectric Spectroscopy. Dielectric spectroscopy measurements of DMAMg/P(VDF−TrFE), AmZn/P(VDF−TrFE), and P(VDF−TrFE) films were performed in a parallel plate capacitor geometry in the 200 Hz to 1 MHz frequency range using a HP 4284A precision LCR meter. The experiments were carried out during cooling at a rate of 1 K/min. Silver electrodes were evaporated on films to ensure good electrical contact. Dielectric properties of DMAMg and AmZn powders were determined using the same LCR meter connected to a custom-made cryostat designed for the powder measurements.

RESULTS AND DISCUSSION

DMAMg/P(VDF−TrFE) Composite. First, we characterized the DMAMg/P(VDF−TrFE) composite film using Raman microscopy. The obtained optical image and corresponding Raman map of a randomly selected area on the composite are presented in Figure 2a,b, respectively. The

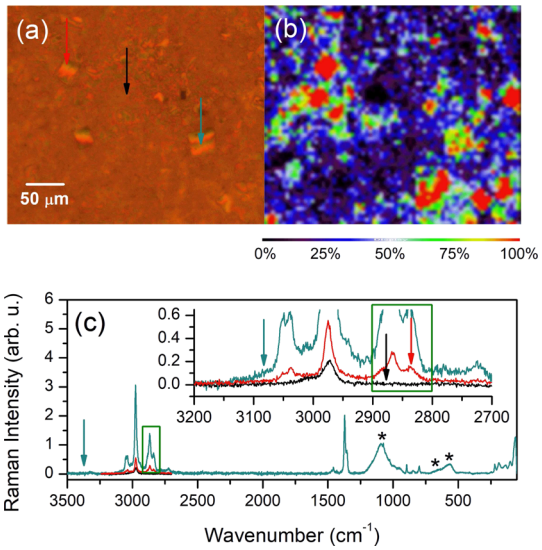

Figure 2. (a) Optical camera image of the mapped area of DMAMg/P(VDF−TrFE) composite. (b) Raman map of the same region generated as the intensity of peak at 2868 cm^{-1} corresponding to the DMA^+ cation. The color scale bar shows a distribution of crystals (red) in the film (black). (c) Full-range Raman spectrum (cyan) of a DMAMg crystallite in the polymer matrix together with the narrow-range spectra taken during the mapping experiment (red and black colors corresponding to DMAMg crystallite and to the P(VDF−TrFE) film, respectively). The spectra were collected from the spots indicated by arrows in the (a) panel. The Raman signal from a cover glass slide is marked with the asterisks. The area marked with the green rectangle was used to generate the intensity map of the peak at 2868 cm^{-1}.

mapping was performed by measuring the intensity of 2868 cm^{-1} Raman line (Figure 2c), which corresponds to the DMAMg compound. The imaging indicates rather moderate homogeneity of the DMAMg filler distribution in the copolymer matrix with the average size of about 20 μm, and size of the biggest crystallites being less than 50 μm. The Raman spectrum of a single DMAMg inclusion agrees perfectly with the expected spectrum of DMAMg (Figure 2c).[50]

We further used dielectric spectroscopy to probe the dielectric properties of this composite film. The temperature dependences of the real ε' and imaginary ε'' parts of the complex dielectric permittivity $\varepsilon^* = \varepsilon' - i\varepsilon''$ of DMAMg/P(VDF−TrFE) are presented in Figure 3. Several partially

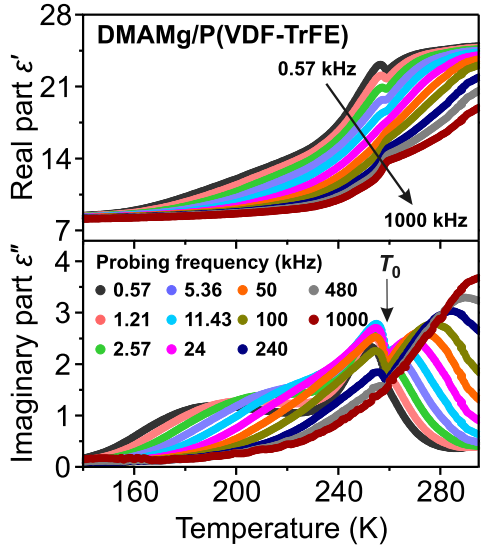

Figure 3. Temperature dependence of the real and imaginary parts of the complex dielectric permittivity of DMAMg/P(VDF−TrFE) composite film probed at different frequencies. T_0 marks the structural phase transition point of DMAMg.

overlapping dipolar relaxations can be identified in the broad temperature range superimposed with the anomalous behavior of ε^* at about 260 K. The low-frequency value of ε' at room temperature is 25, while it decreases to about 8 at 140 K. To separate and identify different relaxation processes of DMAMg/P(VDF−TrFE) composite, we also performed dielectric spectroscopy measurements of pure DMAMg powder and pure P(VDF−TrFE) copolymer film.

Temperature-dependent ε^* of DMAMg powder is presented in Figure 4, revealing a structural phase transition at about 260 K followed by a pronounced dipolar relaxation in a broad temperature range below T_0. The dispersion above the phase transition point is due to the electrical conductivity. The obtained low-frequency value of ε' at room temperature is about 9. However, this value is obtained for a powder sample meaning that ε' of a single crystal should be significantly higher. For comparison, the dielectric constant of a related $[CH_3NH_2NH_2][Zn(HCOO)_3]$ single crystal is above 15 at room temperature,[51,52] while for DMAZn it is about 30.[32] Note that Pato-Doldán et al. reported a very similar dielectric behavior of DMAMg pellets.[26]

The dielectric behavior of the pure P(VDF−TrFE) copolymer film is presented in Figure 5, revealing an onset of the dipolar relaxation above 230 K. The origin of this process is the dipolar glass dynamics due to the glass transition of the noncrystalline regions of the copolymer matrix.[48,49] The obtained low-frequency value of ε' of the P(VDF−TrFE) film without the inclusions is slightly below 13 at room temperature in good agreement with other studies.[48,49] Note that we also performed measurements of this film at higher temperature to detect the ferroelectric phase transition (see Figure S1 in the Supporting Information). The temperature of this phase transition is about 383 K on heating and 348 K on cooling,

DOI: 10.1021/acs.jpcc.9b04235
J. Phys. Chem. C 2019, 123, 16380−16387

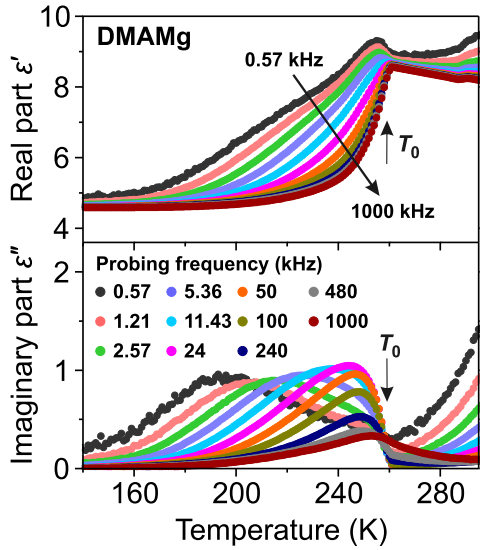

Figure 4. Temperature dependence of the real and imaginary parts of the complex dielectric permittivity of DMAMg powder probed at different frequencies. T_0 marks the structural phase transition point of DMAMg.

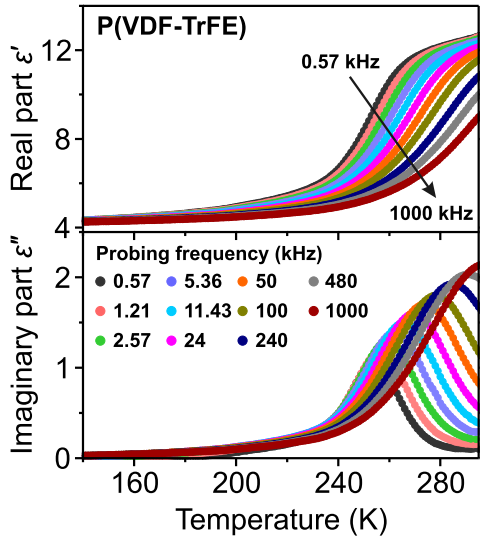

Figure 5. Temperature dependence of the real and imaginary parts of the complex dielectric permittivity of the P(VDF−TrFE) copolymer film probed at different frequencies.

indicating huge temperature hysteresis, which is typical for P(VDF−TrFE) copolymers.[49]

The obtained results of DMAMg powder and pure P(VDF−TrFE) copolymer explain the rich dielectric behavior of the DMAMg/P(VDF−TrFE) composite film presented in Figure 3. The relaxation observed above 260 K clearly originates from the P(VDF−TrFE) film, whereas the low-temperature dynamics are mainly related to the DMAMg inclusions. The anomalous behavior at about 260 K corresponds to the structural phase transition in DMAMg. The dielectric constant of the composite is roughly 2 times higher compared with pure P(VDF−TrFE) film. This enhancement occurs due to the higher dielectric permittivity of the DMAMg fillers, and it is frequently observed for other polymer composites.[45−48]

We further investigated the dipolar relaxation processes in the DMAMg/P(VDF−TrFE) composite, DMAMg powder, and pure P(VDF−TrFE) film by analyzing the frequency dependence of ε^* at different temperature (see Figures S2−S4 in the Supporting Information). Each observed relaxation process was approximated using the empirical Cole−Cole equation[53]

$$\varepsilon^*(\omega) = \varepsilon(\infty) + \frac{\Delta\varepsilon}{1 + (i\omega\tau)^{\alpha}} \quad (1)$$

Here, $\varepsilon(\infty)$ denotes the dielectric permittivity in the high-frequency limit, τ is the mean relaxation time, $\Delta\varepsilon$ is the dielectric strength of the relaxation, and $\omega = 2\pi\nu$ is the angular probing frequency. Parameter $0 \leq \alpha < 1$ determines the width of the relaxation. For $\alpha = 1$, the given equation reduces to the Debye model.[53]

The fits of the data using eq 1 allowed us to obtain the inverse temperature dependence of ln τ for the main dipolar relaxations in DMAMg/P(VDF−TrFE), DMAMg, and P(VDF−TrFE) (see Figure 6). The observed linear behavior for

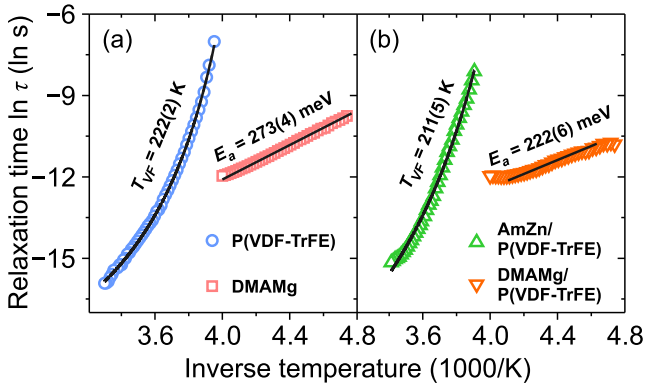

Figure 6. Inverse temperature dependence of the mean relaxation time of different processes in (a) DMAMg framework and pure P(VDF−TrFE) film and (b) both composites. The solid curves are the best fits to the Arrhenius and Vogel−Fulcher equations.

the relaxation of the DMAMg framework indicates the Arrhenius process

$$\tau = \tau_0 \exp(E_a/kT) \quad (2)$$

where E_a and τ_0 denote the activation energy and attempt time, respectively, and k is the Boltzmann constant. For DMAMg powder, we obtained E_a = 273(4) meV and $\tau_0 = 1.7(2) \times 10^{-11}$ s, while for DMAMg in the composite these values are 222(6) meV and $\tau_0 = 1.3(3) \times 10^{-10}$ s. This suggests the effect of the copolymer matrix on the dipolar relaxation of the DMAMg fillers. However, this difference might also originate because of the inability to fully separate the overlapping relaxations of DMAMg and P(VDF−TrFE) copolymer matrix in this temperature region.

Our analysis of the frequency-dependent data also allowed us to study the origin of the dipolar relaxation of DMAMg below T_0. The obtained activation energy of this process is close to the value of 235 meV determined by the ^{1}H NMR spectroscopy for the DMA^+ cation hopping motion in DMAMg.[29] The same NMR investigation also revealed that a substantial fraction of the supercooled disordered phase coexists with the ordered phase down to 220 K, whereas another X-ray diffraction study detected the presence of such a phase even at 170 K.[26] Thus, the likely origin of the dipolar relaxation observed in DMAMg is the DMA^+ cation hopping

DOI: 10.1021/acs.jpcc.9b04235
J. Phys. Chem. C 2019, 123, 16380−16387

dynamics in the disordered fraction of the framework below T_0. Note that in agreement with previous study,[26] we also did not observe DMA^+ dynamics above T_0, as such a process likely becomes too fast in the high-temperature phase to be probed by our frequency range.

The inverse temperature dependence of ln τ for the main relaxation process of P(VDF−TrFE) film significantly deviates from a straight line behavior (Figure 6a). This indicates freezing of the dipolar glass dynamics described by the Vogel−Fulcher law[54]

$$\tau = \tau_0 \exp(E_{VF}/k(T - T_{VF})) \quad (3)$$

where T_{VF} denotes the freezing temperature and E_{VF} has a meaning of energy. The obtained freezing temperature for pure P(VDF−TrFE) copolymer is T_{VF} = 222(2) K, which is in good agreement with previous studies.[45,48] The relaxation process due to the dipolar glass freezing is also observed for the DMAMg/P(VDF−TrFE) composite (see Figure 3). However, because of the overlapping relaxations, a reliable determination of τ is only possible in a relatively narrow temperature range, which is not sufficient to identify the Vogel−Fulcher behavior (not shown).

AmZn/P(VDF−TrFE) Composite. The optical camera image and Raman microscopy map of AmZn/P(VDF−TrFE) film also revealed a moderate homogeneity of AmZn filler distribution in the copolymer matrix, though the average size of the crystallites is slightly bigger than that in DMAMg/P(VDF−TrFE) (see Figure 7). The obtained Raman spectrum from a single AmZn inclusion is in a perfect agreement with the expected pattern for the AmZn framework (Figure 7c).[55]

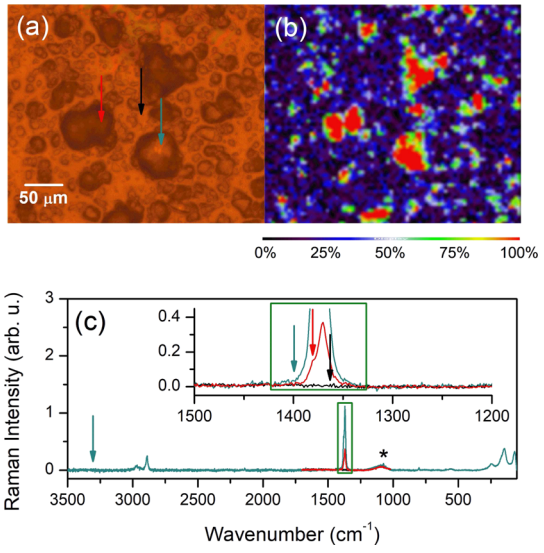

Figure 7. (a) Optical camera image of the mapped area of AmZn/P(VDF−TrFE) composite. (b) Raman map of the same region generated as the intensity of peak at 1370 cm^{-1} corresponding to the Am^+ cation. The color scale bar shows a distribution of crystals (red) in the film (black). (c) Full-range Raman spectrum (cyan) of AmZn crystallite in the polymer matrix together with the narrow-range spectra taken during the mapping experiment (red and black colors corresponding to AmZn crystallite and to the P(VDF−TrFE) film, respectively). The spectra were collected from the spots indicated by arrows in the (a) panel. The Raman signal from a cover glass slide is marked with the asterisks. The area marked with the green rectangle was used to generate the intensity map of the peak at 1370 cm^{-1}.

The temperature dependence of ε^* of the AmZn/P(VDF−TrFE) composite film is presented in Figure 8, revealing the

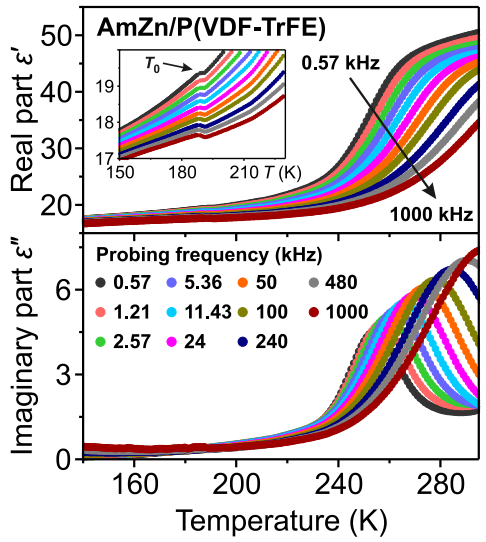

Figure 8. Temperature dependence of the real and imaginary parts of the complex dielectric permittivity of AmZn/P(VDF−TrFE) composite film probed at different frequencies. The inset emphasizes the behavior of ε' about the phase transition point of AmZn. T_0 marks the structural phase transition point of AmZn.

same dipolar relaxation above 230 K as observed for pure P(VDF−TrFE) copolymer (compare with Figure 5). The dielectric permittivity of the composite is about four times higher, indicating fillers of relatively high ε'. In addition, a small anomaly of ε^* is observed at about 188 K (see inset in Figure 8).

To elucidate the dielectric behavior of the AmZn/P(VDF−TrFE) composite, we also performed temperature-dependent dielectric measurements of AmZn powder (Figure 9). The obtained behavior of ε^* at higher temperature is mainly

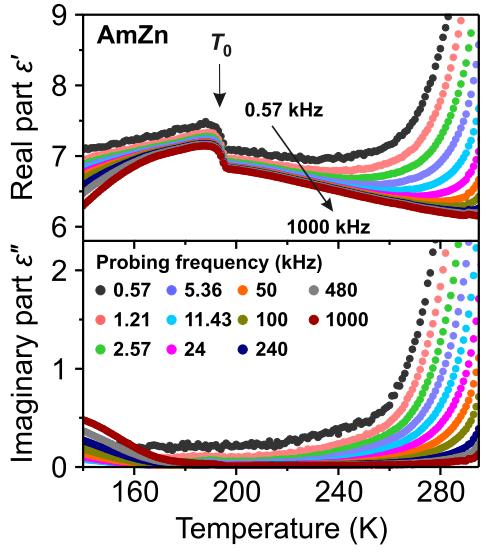

Figure 9. Temperature dependence of the real and imaginary parts of the complex dielectric permittivity of AmZn powder probed at different frequency. T_0 marks the structural phase transition point of AmZn.

DOI: 10.1021/acs.jpcc.9b04235
J. Phys. Chem. C 2019, 123, 16380−16387

influenced by the electrical conductivity. At low temperature, the conductivity effects are absent, and the low-frequency value of ε' is slightly above 7, which is higher compared to that of the pure P(VDF−TrFE) copolymer film. The powder nature of our sample indicates that ε' of a single crystal must be even higher, explaining the significant dielectric permittivity enhancement of AmZn/P(VDF−TrFE) composite. In addition, the real part of the dielectric permittivity exhibits a clear anomaly at about 188 K, which is caused by the ferroelectric phase transition of AmZn. Note that because of the powder nature of our measurements, the observed value of ε' at the phase transition point is significantly smaller compared with the single-crystal measurements performed along the polar axis of this compound.[12]

The suppressed phase transition anomaly observed for AmZn/P(VDF−TrFE) film can be qualitatively explained using the Lichtenecker model designed to calculate the dielectric permittivity of various composites[56]

$$(\varepsilon')^{\beta} = (1 - x)(\varepsilon_1')^{\beta} + x(\varepsilon_2')^{\beta} \quad (4)$$

Here, x is a filler fraction in the composite and $-1 \leq \beta \leq 1$ describes the spatial distribution of both phases. In our case, ε_1' and ε_2' denote the dielectric constants of P(VDF−TrFE) copolymer and AmZn framework, respectively. The positive value of β indicates percolation of the fillers, whereas $\beta < 0$ occurs for nonpercolating composites.[57] For a sufficiently negative value of β, the dielectric permittivity anomalies can be significantly suppressed, though the overall enhancement of ε' is maintained. A similar situation is observed for AmZn/P(VDF−TrFE) and DMAMg/P(VDF−TrFE) composites.

We further used the Cole−Cole relaxation model to approximate the dipolar glass dynamics of the copolymer matrix of the AmZn/P(VDF−TrFE) film (see Figure S5). As for pure P(VDF−TrFE), the inverse temperature dependence of the mean relaxation time also follows the Vogel−Fulcher law with T_{VF} = 211(5) K (see Figure 6b). This indicates an almost negligible effect of the AmZn inclusions on the glassy properties of P(VDF−TrFE).

The temperature-dependent ε'' of the AmZn/P(VDF−TrFE) composite also reveals another weakly expressed dipolar relaxation below the phase transition point. The same process is clearly visible in the dielectric measurements of AmZn powder (Figure 9). However, our experimental temperature range is too narrow to reliably estimate the activation energy of this relaxation obscuring identification of its origin.

SUMMARY AND CONCLUSIONS

In summary, we reported the preparation and spectroscopic characterization of P(VDF−TrFE)-based composite films containing DMAMg (23 wt %) and AmZn (17 wt %) formate frameworks. The Raman microscopy was used to map the morphology of both composites, demonstrating moderate homogeneity of the MOF filler distribution.

The dielectric spectroscopy experiments of the DMAMg/P(VDF−TrFE) film revealed rich dielectric behavior in a broad temperature range. The origin of the observed dipolar relaxations and dielectric anomaly was elucidated by performing measurements of the pure P(VDF−TrFE) copolymer film and DMAMg powder. We found that the relaxation at higher temperature occurs because of the dipolar glass freezing of the P(VDF−TrFE) matrix, while the dipolar process detected at lower temperature can be assigned to the DMA^+ cation dynamics. The anomalous behavior of the dielectric permittivity at about 260 K was attributed to the structural phase transition of the DMAMg framework. The determined activation energy of the DMA^+ cation motion is slightly smaller in DMAMg/P(VDF−TrFE), which may suggest the influence of the polymer matrix on the formate framework. However, the overlap of both relaxations in the composite may also account for this discrepancy. We also observed a substantial increase of the dielectric permittivity of the composite film compared to pure P(VDF−TrFE).

We observed that the dielectric properties of AmZn/P(VDF−TrFE) film are mainly determined by the dipolar glass freezing dynamics of the copolymer matrix. The determined freezing temperature is close to that of the pure P(VDF−TrFE), indicating a negligible effect of the fillers on the polymer matrix. The small phase transition anomaly of AmZn was also detected at about 188 K, which is in a perfect agreement with the AmZn powder measurements. For this composite, we also detected a significant increase of the dielectric permittivity upon AmZn filler addition, which can be qualitatively explained using the Lichtenecker model.

To our knowledge, the presented work is a first report of the composite films based on the polymer matrix with embedded metal−formate frameworks. The choice of the components of the studied composites was mainly driven by their rich dielectric behavior, though we expect that other polymers (e.g., polyvinylidene fluoride−trifluoroethylene−chlorofluoroethylene terpolymer[58]) and dense MOFs may provide comparable or even better properties with pronounced synergy effects. We anticipate that the reported and similar composites might significantly enhance the stability and potential applicability of the formate frameworks, which exhibit peculiar dielectric (ferroelectric) and multiferroic properties. This also demands further dielectric studies of these composites with different filler concentrations and measurements of the pyroelectric and ferroelectric response.

REFERENCES

ASSOCIATED CONTENT

Supporting Information

The Supporting Information is available free of charge on the ACS Publications website at DOI: 10.1021/acs.jpcc.9b04235.

Additional experimental data of dielectric spectroscopy (PDF)

AUTHOR INFORMATION

Corresponding Author

*E-mail: mantas.simenas@ff.vu.lt. Phone: +370 5 2234537. Fax: +370 5 2234537.

ORCID

Mantas Šimėnas: 0000-0002-2733-2270

Monique A. van der Veen: 0000-0002-0316-4639

Notes

The authors declare no competing financial interest.

ACKNOWLEDGMENTS

This work was supported by the Research Council of Lithuania (Project TAP LLT-4/2017). The work of A.G.-N. forms part of the research program of DPI, project #731.015.506.

DOI: 10.1021/acs.jpcc.9b04235
J. Phys. Chem. C 2019, 123, 16380−16387

M.A.v.d.V. thanks the European Research council for ERC-Starting grant no 759212.

REFERENCES

(1) Kitagawa, S.; Kitaura, R.; Noro, S.-i. Functional Porous Coordination Polymers. *Angew. Chem., Int. Ed.* **2004**, *43*, 2334−2375.

(2) Rosseinsky, M. J. Recent Developments in Metal-Organic Framework Chemistry: Design, Discovery, Permanent Porosity and Flexibility. *Microporous Mesoporous Mater.* **2004**, *73*, 15−30.

(3) Meek, S. T.; Greathouse, J. A.; Allendorf, M. D. Metal-Organic Frameworks: A Rapidly Growing Class of Versatile Nanoporous Materials. *Adv. Mater.* **2011**, *23*, 249−267.

(4) Kuppler, R. J.; Timmons, D. J.; Fang, Q.-R.; Li, J.-R.; Makal, T. A.; Young, M. D.; Yuan, D.; Zhao, D.; Zhuang, W.; Zhou, H.-C. Potential Applications of Metal-Organic Frameworks. *Coord. Chem. Rev.* **2009**, *253*, 3042−3066.

(5) He, Y.; Zhou, W.; Qian, G.; Chen, B. Methane Storage in Metal-Organic Frameworks. *Chem. Soc. Rev.* **2014**, *43*, 5657−5678.

(6) Murray, L. J.; Dincă, M.; Long, J. R. Hydrogen Storage in Metal-Organic Frameworks. *Chem. Soc. Rev.* **2009**, *38*, 1294−1314.

(7) Li, J.-R.; Sculley, J.; Zhou, H.-C. Metal-Organic Frameworks for Separations. *Chem. Rev.* **2012**, *112*, 869−932.

(8) Wu, M.-X.; Yang, Y.-W. Metal-Organic Framework (MOF)-Based Drug/Cargo Delivery and Cancer Therapy. *Adv. Mater.* **2017**, *29*, 1606134.

(9) Cheetham, A. K.; Rao, C. N. R. There's Room in the Middle. *Science* **2007**, *318*, 58−59.

(10) Jain, P.; Dalal, N. S.; Toby, B. H.; Kroto, H. W.; Cheetham, A. K. Order-Disorder Antiferroelectric Phase Transition in a Hybrid Inorganic-Organic Framework with the Perovskite Architecture. *J. Am. Chem. Soc.* **2008**, *130*, 10450−10451.

(11) Jain, P.; Ramachandran, V.; Clark, R. J.; Zhou, H. D.; Toby, B. H.; Dalal, N. S.; Kroto, H. W.; Cheetham, A. K. Multiferroic Behavior Associated with an Order-Disorder Hydrogen Bonding Transition in Metal-Organic Frameworks (MOFs) with the Perovskite ABX_3 Architecture. *J. Am. Chem. Soc.* **2009**, *131*, 13625−13627.

(12) Xu, G.-C.; Ma, X.-M.; Zhang, L.; Wang, Z.-M.; Gao, S. Disorder-Order Ferroelectric Transition in the Metal Formate Framework of $[NH_4][Zn(HCOO)_3]$. *J. Am. Chem. Soc.* **2010**, *132*, 9588−9590.

(13) Du, Z.-Y.; Xu, T.-T.; Huang, B.; Su, Y.-J.; Xue, W.; He, C.-T.; Zhang, W.-X.; Chen, X.-M. Switchable Guest Molecular Dynamics in a Perovskite-Like Coordination Polymer toward Sensitive Thermoresponsive Dielectric Materials. *Angew. Chem., Int. Ed.* **2015**, *54*, 914−918.

(14) Wu, Y.; Shaker, S.; Brivio, F.; Murugavel, R.; Bristowe, P. D.; Cheetham, A. K. $[Am]Mn(H_2POO)_3$: A New Family of Hybrid Perovskites Based on the Hypophosphite Ligand. *J. Am. Chem. Soc.* **2017**, *139*, 16999−17002.

(15) Mączka, M.; Gągor, A.; Ptak, M.; Paraguassu, W.; da Silva, T. A.; Sieradzki, A.; Pikul, A. Phase Transitions and Coexistence of Magnetic and Electric Orders in the Methylhydrazinium Metal Formate Frameworks. *Chem. Mater.* **2017**, *29*, 2264−2275.

(16) Asaji, T.; Ashitomi, K. Phase Transition and Cationic Motion in a Metal-Organic Perovskite, Dimethylammonium Zinc Formate $[(CH_3)_2NH_2][Zn(HCOO)_3]$. *J. Phys. Chem. C* **2013**, *117*, 10185−10190.

(17) Šimėnas, M.; Ptak, M.; Khan, A. H.; Dagys, L.; Balevičius, V.; Bertmer, M.; Völkel, G.; Mączka, M.; Pöppl, A.; Banys, J. Spectroscopic Study of $[(CH_3)_2NH_2][Zn(HCOO)_3]$ Hybrid Perovskite Containing Different Nitrogen Isotopes. *J. Phys. Chem. C* **2018**, *122*, 10284−10292.

(18) Sánchez-Andújar, M.; Presedo, S.; Yánez-Vilar, S.; Castro-García, S.; Shamir, J.; Senarís-Rodríguez, M. A. Characterization of the Order-Disorder Dielectric Transition in the Hybrid Organic-Inorganic Perovskite-Like Formate $Mn(HCOO)_3[(CH_3)_2NH_2]$. *Inorg. Chem.* **2010**, *49*, 1510−1516.

(19) Tian, Y.; Stroppa, A.; Chai, Y.; Yan, L.; Wang, S.; Barone, P.; Picozzi, S.; Sun, Y. Cross Coupling between Electric and Magnetic Orders in a Multiferroic Metal-Organic Framework. *Sci. Rep.* **2014**, *4*, 6062.

(20) Šimėnas, M.; Balčiūnas, S.; Mączka, M.; Banys, J.; Tornau, E. E. Structural Phase Transition in Perovskite Metal-Formate Frameworks: a Potts-Type Model with Dipolar Interactions. *Phys. Chem. Chem. Phys.* **2016**, *18*, 18528−18535.

(21) Jain, P.; Stroppa, A.; Nabok, D.; Marino, A.; Rubano, A.; Paparo, D.; Matsubara, M.; Nakotte, H.; Fiebig, M.; Picozzi, S.; et al. Switchable Electric Polarization and Ferroelectric Domains in a Metal-Organic-Framework. *npj Quantum Mater.* **2016**, *1*, 16012.

(22) Fu, D.-W.; Zhang, W.; Cai, H.-L.; Zhang, Y.; Ge, J.-Z.; Xiong, R.-G.; Huang, S. D.; Nakamura, T. A Multiferroic Perdeutero Metal-Organic Framework. *Angew. Chem., Int. Ed.* **2011**, *50*, 11947−11951.

(23) Wang, X.-Y.; Gan, L.; Zhang, S.-W.; Gao, S. Perovskite-like Metal Formates with Weak Ferromagnetism and as Precursors to Amorphous Materials. *Inorg. Chem.* **2004**, *43*, 4615−4625.

(24) Xu, G.-C.; Zhang, W.; Ma, X.-M.; Chen, Y.-H.; Zhang, L.; Cai, H.-L.; Wang, Z.-M.; Xiong, R.-G.; Gao, S. Coexistence of Magnetic and Electric Orderings in the Metal-Formate Frameworks of $[NH_4][M(HCOO)_3]$. *J. Am. Chem. Soc.* **2011**, *133*, 14948−14951.

(25) Eerenstein, W.; Mathur, N. D.; Scott, J. F. Multiferroic and Magnetoelectric Materials. *Nature* **2006**, *442*, 759−765.

(26) Pato-Doldán, B.; Sánchez-Andújar, M.; Gómez-Aguirre, L. C.; Yáñez-Vilar, S.; López-Beceiro, J.; Gracia-Fernández, C.; Haghighirad, A. A.; Ritter, F.; Castro-García, S.; Señarís-Rodríguez, M. A. Near Room Temperature Dielectric Transition in the Perovskite Formate Framework $[(CH_3)_2NH_2][Mg(HCOO)_3]$. *Phys. Chem. Chem. Phys.* **2012**, *14*, 8498−8501.

(27) Sletten, E.; Jensen, L. H. The Crystal Structure of Dimethylammonium Copper(II) Formate, $NH_2(CH_2)_2[Cu(OOCH)_3]$. *Acta Crystallogr., Sect. B: Struct. Crystallogr. Cryst. Chem.* **1973**, *29*, 1752−1756.

(28) Rossin, A.; Ienco, A.; Costantino, F.; Montini, T.; Di Credico, B.; Caporali, M.; Gonsalvi, L.; Fornasiero, P.; Peruzzini, M. Phase Transitions and CO_2 Adsorption Properties of Polymeric Magnesium Formate. *Cryst. Growth Des.* **2008**, *8*, 3302−3308.

(29) Asaji, T.; Yoshitake, S.; Ito, Y.; Fujimori, H. Phase Transition and Cationic Motion in the Perovskite Formate Framework $[(CH_3)_2NH_2][Mg(HCOO)_3]$. *J. Mol. Struct.* **2014**, *1076*, 719−723.

(30) Szafrański, M.; Wei, W.-J.; Wang, Z.-M.; Li, W.; Katrusiak, A. Research Update: Tricritical Point and Large Caloric Effect in a Hybrid Organic-Inorganic Perovskite. *APL Mater.* **2018**, *6*, 100701.

(31) Šimėnas, M.; Kultaeva, A.; Balčiūnas, S.; Trzebiatowska, M.; Klose, D.; Jeschke, G.; Mączka, M.; Banys, J.; Pöppl, A. Single Crystal Electron Paramagnetic Resonance of Dimethylammonium and Ammonium Hybrid Formate Frameworks: Influence of External Electric Field. *J. Phys. Chem. C* **2017**, *121*, 16533−16540.

(32) Šimėnas, M.; Balčiūnas, S.; Ciupa, A.; Vilčiauskas, L.; Jablonskas, D.; Kinka, M.; Sieradzki, A.; Samulionis, V.; Mączka, M.; Banys, J. Elucidation of Dipolar Dynamics and the Nature of Structural Phases in the $[(CH_3)_2NH_2][Zn(HCOO)_3]$ Hybrid Perovskite Framework. *J. Mater. Chem. C* **2019**, *7*, 6779.

(33) Liang, X.; Zhang, F.; Feng, W.; Zou, X.; Zhao, C.; Na, H.; Liu, C.; Sun, F.; Zhu, G. From Metal-Organic Framework (MOF) to MOF-Polymer Composite Membrane: Enhancement of Low-Humidity Proton Conductivity. *Chem. Sci.* **2013**, *4*, 983−992.

(34) Zhang, Y.; Feng, X.; Yuan, S.; Zhou, J.; Wang, B. Challenges and Recent Advances in MOF-Polymer Composite Membranes for Gas Separation. *Inorg. Chem. Front.* **2016**, *3*, 896−909.

(35) Calvez, C. L.; Zouboulaki, M.; Petit, C.; Peeva, L.; Shirshova, N. One Step Synthesis of MOF-polymer Composites. *RSC Adv.* **2016**, *6*, 17314−17317.

(36) Dechnik, J.; Sumby, C. J.; Janiak, C. Enhancing Mixed-Matrix Membrane Performance with Metal-Organic Framework Additives. *Cryst. Growth Des.* **2017**, *17*, 4467−4488.

(37) Pastore, V. J.; Cook, T. R.; Rzayev, J. Polymer-MOF Hybrid Composites with High Porosity and Stability through Surface-Selective Ligand Exchange. *Chem. Mater.* **2018**, *30*, 8639−8649.

DOI: 10.1021/acs.jpcc.9b04235
J. Phys. Chem. C 2019, 123, 16380−16387

(38) Dong, G.; Li, H.; Chen, V. Challenges and Opportunities for Mixed-Matrix Membranes for Gas Separation. *J. Mater. Chem. A* **2013**, *1*, 4610−4630.
(39) Denny, M. S., Jr.; Cohen, S. M. In Situ Modification of Metal-Organic Frameworks in Mixed-Matrix Membranes. *Angew. Chem., Int. Ed.* **2015**, *54*, 9029−9032.
(40) Feijani, E. A.; Mahdavi, H.; Tavasoli, A. Poly(Vinylidene Fluoride) Based Mixed Matrix Membranes Comprising Metal Organic Frameworks for Gas Separation Applications. *Chem. Eng. Res. Des.* **2015**, *96*, 87−102.
(41) Li, W.; Meng, Q.; Zhang, C.; Zhang, G. Metal-Organic Framework/PVDF Composite Membranes with High H_2 Permselectivity Synthesized by Ammoniation. *Chem.—Eur. J.* **2015**, *21*, 7224−7230.
(42) Feijani, E. A.; Mahdavi, H.; Tavassoli, A. Synthesis and Gas Permselectivity of CuBTC-GO-PVDF Mixed Matrix Membranes. *New J. Chem.* **2018**, *42*, 12013−12023.
(43) Tan, Y.; Sun, Z.; Meng, H.; Han, Y.; Wu, J.; Xu, J.; Xu, Y.; Zhang, X. A New MOFs/Polymer Hybrid Membrane: MIL-68(Al)/PVDF, Fabrication and Application in High-Efficient Removal of p-Nitrophenol and Methylene Blue. *Sep. Purif. Technol.* **2019**, *215*, 217−226.
(44) Shvartsman, V. V.; Kiselev, D. A.; Solnyshkin, A. V.; Lupascu, D. C.; Silibin, M. V. Evolution of Poled State in P(VDF−TrFE)/(Pb,Ba)(Zr,Ti)O_3 Composites Probed by Temperature Dependent Piezoresponse and Kelvin Probe Force Microscopy. *Sci. Rep.* **2018**, *8*, 378.
(45) Hilczer, B.; Kułek, J.; Markiewicz, E.; Kosec, M.; Malič, B. Dielectric Relaxation in Ferroelectric PZT-PVDF Nanocomposites. *J. Non-Cryst. Solids* **2002**, *305*, 167−173.
(46) Belovickis, J.; Samulionis, V.; Banys, J.; Silibin, M.; Solnyshkin, A.; Shilyaeva, Y.; Nekludov, K.; Gavrilov, S.; Rubanik, V.; Rubanik, V.; et al. Ultrasonic Spectroscopy of Copolymer Based P(VDF−TrFE) Composites with Fillers on Lead Zirconate Titanate Basis. *Polym. Test.* **2016**, *53*, 211−216.
(47) Zhang, W. L.; Yu, Y. C.; Luo, W. B.; Shuai, Y.; Pan, X. Q.; Wu, Q. Q.; Wu, C. G. Lead Free KNN/P(VDF−TrFE) 0-3 Pyroelectric Composite Films and Its Infrared Sensor. *Infrared Phys. Technol.* **2017**, *80*, 100−104.
(48) Belovickis, J.; Ivanov, M.; Svirskas, Š.; Samulionis, V.; Banys, J.; Solnyshkin, A. V.; Gavrilov, S. A.; Nekludov, K. N.; Shvartsman, V. V.; Silibin, M. V. Dielectric, Ferroelectric, and Piezoelectric Investigation of Polymer-Based P(VDF−TrFE) Composites. *Phys. Status Solidi B* **2018**, *255*, 1700196.
(49) Furukawa, T.; Tajitsu, Y.; Zhang, X.; Johnson, G. E. Dielectric Relaxations in Copolymers of Vinylidene Fluoride. *Ferroelectrics* **1992**, *135*, 401−417.
(50) Szymborska-Małek, K.; Trzebiatowska-Gusowska, M.; Mączka, M.; Gągor, A. Temperature-Dependent IR and Raman Studies of Metal-Organic Frameworks $[(CH_3)_2NH_2][M(HCOO)_3]$, M=Mg and Cd. *Spectrochim. Acta, Part A* **2016**, *159*, 35−41.
(51) Šimėnas, M.; Balčiūnas, S.; Trzebiatowska, M.; Ptak, M.; Mączka, M.; Völkel, G.; Pöppl, A.; Banys, J. Electron Paramagnetic Resonance and Electric Characterization of a $[CH_3NH_2NH_2][Zn(HCOO)_3]$ Perovskite Metal Formate Framework. *J. Mater. Chem. C* **2017**, *5*, 4526−4536.
(52) Sieradzki, A.; Mączka, M.; Simenas, M.; Zaręba, J. K.; Gągor, A.; Balciunas, S.; Kinka, M.; Ciupa, A.; Nyk, M.; Samulionis, V.; et al. On the Origin of Ferroelectric Structural Phases in Perovskite-Like Metal-Organic Formate. *J. Mater. Chem. C* **2018**, *6*, 9420−9429.
(53) Schonhals, A.; Kremer, F. *Broadband Dielectric Spectroscopy*, 1st ed.; Springer-Verlag Berlin Heidelberg, 2003.
(54) Trachenko, K. The Vogel-Fulcher-Tammann Law in the Elastic Theory of Glass Transition. *J. Non-Cryst. Solids* **2008**, *354*, 3903−3906.
(55) Mączka, M.; Kadlubanski, P.; Freire, P. T. C.; Macalik, B.; Paraguassu, W.; Hermanowicz, K.; Hanuza, J. Temperature- and Pressure-Induced Phase Transitions in the Metal Formate Framework of $[ND_4][Zn(DCOO)_3]$ and $[NH_4][Zn(HCOO)_3]$. *Inorg. Chem.* **2014**, *53*, 9615−9624.
(56) Goncharenko, A. V.; Lozovski, V. Z.; Venger, E. F. Lichtenecker's Equation: Applicability and Limitations. *Opt. Commun.* **2000**, *174*, 19−32.
(57) Petzelt, J.; Nuzhnyy, D. Broadband Dielectric Spectroscopy of Inhomogeneous and Composite Weak Conductors. *Phase Transitions* **2016**, *89*, 651−666.
(58) Xia, F.; Cheng, Z.-Y.; Xu, H. S.; Li, H. F.; Zhang, Q. M.; Kavarnos, G. J.; Ting, R. Y.; Abdul-Sadek, G.; Belfield, K. D. High Electromechanical Responses in a Poly(vinylidene fluoride-trifluoroethylene-chlorofluoroethylene) Terpolymer. *Adv. Mater.* **2002**, *14*, 1574−1577.

DOI: 10.1021/acs.jpcc.9b04235
J. Phys. Chem. C 2019, 123, 16380−16387